New Journal of Physics
The open access journal at the forefront of physics

Deutsche Physikalische Gesellschaft DPG
IOP Institute of Physics

Published in partnership with: Deutsche Physikalische Gesellschaft and the Institute of Physics

OPEN ACCESS

RECEIVED
29 April 2021

REVISED
29 July 2021

ACCEPTED FOR PUBLICATION
5 August 2021

PUBLISHED
27 August 2021

PAPER

Quantum sensing protocol for motionally chiral Rydberg atoms

S Y Buhmann[1,*], S M Giesen[2], M Diekmann[2], R Berger[2], S Aull[1], P Zahariev[1,3], M Debatin[1] and K Singer[1,*]

[1] Institut für Physik, Universität Kassel, Heinrich-Plett-Str. 40, 34132 Kassel, Germany
[2] Fachbereich Chemie, Philipps-Universität Marburg, Hans-Meerwein-Str 4, Marburg 35032, Germany
[3] Institute of Solid State Physics, Bulgarian Academy of Sciences, 72, Tzarigradsko Chaussee, 1784 Sofia, Bulgaria
[*] Authors to whom correspondence should be addressed.

E-mail: stefan.buhmann@physik.uni-freiburg.de and ks@uni-kassel.de

Keywords: Rydberg atoms, quantum sensor, chiral mirror

Abstract

A quantum sensing protocol is proposed for demonstrating the motion-induced chirality of circularly polarised Rydberg atoms. To this end, a cloud of Rydberg atoms is dressed by a bichromatic light field. This allows to exploit the long-lived ground states for implementing a Ramsey interferometer in conjunction with a spin echo pulse sequence for refocussing achiral interactions. Optimal parameters for the dressing lasers are identified. Combining a circularly polarised dipole transition in the Rydberg atom with atomic centre-of-mass motion, the system becomes chiral. The resulting discriminatory chiral energy shifts induced by a chiral mirror are estimated using a macroscopic quantum electrodynamics approach. The presented quantum sensing protocol will also provide an indirect proof for Casimir–Polder quantum friction.

1. Introduction

We propose a method for inducing and detecting chirality in Rydberg atoms by combining circular dipole transitions with centre-of-mass motion. The scheme is based on measuring the dispersion interaction of this artificial chiral system with a chiral mirror which preserves the handedness of circularly polarised light upon reflection. The predicted discriminatory interaction is a leading-order relativistic quantum electrodynamics effect.

Rydberg atoms in conjunction with dressing represent a formidable quantum information platform [1, 2] and quantum sensor due to interaction-induced energy shifts caused by externally applied fields [3] and nearby particles such as molecules. We suggest to use dressed Rydberg atoms as sensitive quantum sensors [4] for chirality exploiting the long lifetimes of sensitive Rydberg states and accurate ground states featured in the hyperfine manifold of the electronic ground state of alkali metals, which are the basis of the current definition of time. Using two-photon dressing from one of the hyperfine levels of the electronic ground states to a Rydberg state we can combine an accurate reference with a sensitive Rydberg state such that interaction-induced energy shifts [5–7] are not probed directly by spectroscopy on the Rydberg state [8–10] but are translated to energy shifts of the ground states. Employing a Ramsey [11] sensing sequence (figure 1) these energy shifts can be accurately determined down to a few tens of milli hertz [12].

Dispersive energy shift in atoms may arise from their interaction with polarisable objects such as molecules [13, 14] or surfaces [14, 15]. Linear-response or macroscopic quantum electrodynamics frameworks allow to consider objects of arbitrary shapes and materials [16–18]. A range of different materials has been considered both for Casimir–Polder and the closely related Casimir interaction [19], including magnetoelectric metamaterials [20–22], chiral objects [23–26], or topological insulators [27–29]. Rydberg atoms with their large electric transition dipole moments [30, 31] are particularly susceptible to dispersive energy shifts. For this reason, they where instrumental in both the first experimental verification of the retarded Casimir–Polder interaction of atoms [32] and the later demonstration of thermal effects in this interaction [33]. On the theory side, it has been shown that the long wavelength of photons arising from neighbouring Rydberg-level transitions can render Casimir–Polder forces due to good conductors

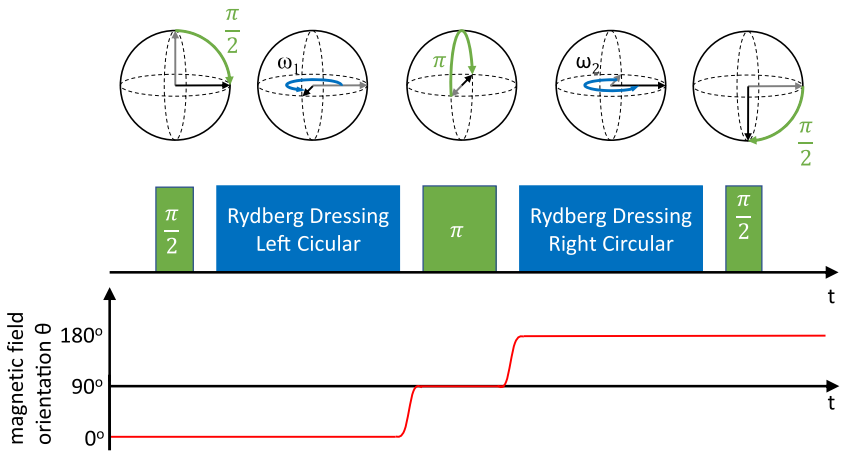

Figure 1. Quantum-sensing protocol for detecting chirality: the Bloch sphere is used for the two stretched states in the electronic ground-state hyperfine manifold of ^{87}Rb split by 6.8 GHz. The north pole denotes the stretched excited hyperfine state in the ground state manifold $5^2S_{1/2}, F = 2, m_F = 2$ and the south pole the stretched ground state $5^2S_{1/2}, F = 1, m_F = 1$. Microwave manipulation is depicted in green, dressing lasers (blue) are switched in circularity after a central spin echo pulse (green). A continuous chiral influence reveals the motional chirality of the Rydberg atoms due to phase shifts $\omega = \omega_1 = -\omega_2$ caused by the chiral environment. Due to the spin echo pulse the resulting phase determined with the overall Ramsey sequence thus is 2ω. The quantization axis depicted by the red curve is defined by a small magnetic field which is adiabatically rotated by 90 degrees after the first Rydberg dressing laser is switched off right before the central spin echo pulse. After that pulse the quantization axis is again rotated such that it points in the opposite direction with regard to the initial orientation.

almost independent of temperature [34] and that the extreme size of Rydberg states leads to multipole contributions particularly at small separations [35]. Recent works proposed sensitive probing of Rydberg-surface interactions via electromagnetically induced transparency [36], predicted that surface-induced Casimir–Polder interactions can lead to the formation of Rydberg dimers [37], and even suggested that Rydberg atoms could be used as sensors for the dynamical Casimir effect [38].

To induce chirality in an achiral Rydberg atom, we combine a circularly polarised dipole transition of the Rydberg atom with atomic centre-of-mass motion. When the time-reversal odd axial vector representing the circular dipole transition has a nonzero component along the time-reversal-odd polar centre-of-mass velocity, the combined system becomes time-reversal even and parity odd, thus realizing true chirality according to Barron [39]. Attempts to utilize such motionally chiral Rydberg atoms to detect an asymmetry in the charge transfer reaction to chiral molecules have been reported, but remained unsuccessful [40]. Herein instead, we propose to detect the resulting enantiodiscriminatory dispersion interaction due to fluctuating fields of a nearby mirror, which is analogous to predicted enantiodiscriminatory optical forces induced by real fields [41, 42].

The envisioned chiral nature of the motion-induced atom-surface interaction is closely related to the conjectured quantum friction, a dissipative quantum vacuum effect that should decelerate the motion of two perfectly smooth dielectric or metal plates moving parallel to each other [43]. The dearth of experimental observations has allowed for debates to flourish regarding existence and velocity-dependence of quantum friction driven by quantum fluctuations even at zero temperature [44, 45]. The proposed measurement scheme in this paper does not only show motion induced chirality but will also provide an indirect proof for Casimir–Polder quantum friction. This is caused by a moving dipole with quantum fluctuations that has been considered as accessible to measurements: here, an atom moves parallel to a surface [46–48]. We have argued that the respective velocity-dependent force stems from three main components: velocity-dependent energy shifts, Röntgen coupling of the moving dipole, and a Doppler effect [49]. The first of these can thus serve as indirect evidence for detecting quantum friction [50]. For linearly polarised dipoles, velocity-dependent shifts only arise for motion towards or away from the plate due to the symmetry of the problem [49]. The chiral shifts considered in this work break this symmetry, enabling velocity-dependent shifts for motion parallel to the surface, which is much easier to implement experimentally. Indeed, it has recently been proposed to indirectly detect Casimir–Polder quantum friction by measurements of geometric phase induced in a quantum dot suspended above a rotating disk [51].

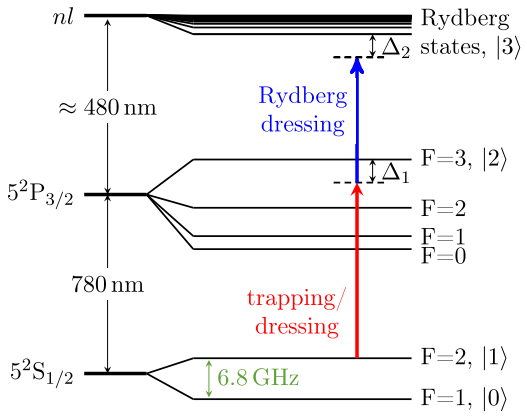

Figure 2. Level scheme of 87-Rubidium (not to scale). $|0\rangle$ is the $5^2S_{1/2}, F = 1, m_F = 1$ ground state serving as reference, $|1\rangle$ is the $5^2S_{1/2}, F = 2, m_F = 2$ launch state which is dressed by a two colour two photon excitation scheme using σ_+ polarisation coupling to the intermediate state $|2\rangle$ and the Rydberg state $|3\rangle$. Laser intensities will be given in terms of one photon resonant Rabi-frequencies Ω_{12} and Ω_{23} for the 780 nm laser and 480 nm laser respectively. Intermediate states different to the $5^2P_{3/2}, F = 3$ states are uncoupled due to the use of circular polarised light the choice of the $m_F = 2$ state in the launch state.

2. Quantum sensing protocol

In the following paragraphs, we will introduce a protocol for sensing energy shifts of Rydberg states using a Ramsey-sequence type of measurement (see figure 1), in which we assume that state-changing collision rates are less than $1/s$. The quantum sensing protocol is exemplified with Rubidium 87 atoms where we start optical pumping all population into the launch state $|1\rangle$ ($5^2S_{1/2}, F = 2, m_F = 2$ see figure 2) with σ_+ polarised light directed along the quantization axis determined by a small magnetic field with its magnitude larger than typical slow external magnetic field drifts. The choice of states avoids state mixing during the two-photon dressing as only the $5^2P_{3/2}, F = 3, m_F = 3$ is coupled due to dipole selection rules. As can be seen in figure 1, the measurement Ramsey sequence is initiated by a $\pi/2$ pulse on the electronic ground state hyperfine manifold ($|0\rangle$, $|1\rangle$) of ^{87}Rb which brings the state in an superposition of $5^2S_{1/2}, F = 1$, $m_F = 1$ and $5^2S_{1/2}, F = 2$, $m_F = 2$ states (see figure 2 for a sketch of the relevant level scheme). A subsequent two-photon dressing laser with circularly polarised light is coupling the interaction induced energy shifts on the Rydberg atom caused by the chiral mirror δ_{RM} (see equation (1)) caused by chiral systems to the upper ground state ($5^2S_{1/2}, F = 2$). Detuning and Rabi-frequency of the dressing lasers are chosen to optimize the energy shift and coherence properties (see below). Then after switching the dressing lasers off, the quantization axis given by the magnetic field is rotated by 90 degrees adiabatically. Subsequently, a spin echo is implemented by a π pulse resonant to the hyperfine-splitting in the ground state and used to refocus all interactions caused by achiral influences from the environment, such that only enantiodiscriminatory signals are detected. Then the quantization axis given by the magnetic field is again rotated adiabatically such that it is in the opposite direction with regard to the initial quantization axis. For the signal caused by the interaction with chiral systems to persist, the circularity of the dressing lasers is switched. The final $\pi/2$ pulse on the hyperfine-levels of the ground state transfers the phase shifts ω_1 and ω_2 caused by the chiral environment into a measurable signal. As the magnitude of the magnetic field is chosen to be larger than any external magnetic field drifts, the spin echo also refocuses those drifts. Also the microwave pulses can be augmented by composite pulses allowing for robust rotations in the ground state manifold [52]. By scanning the duration of the exposure of the atom with the dressing lasers, Ramsey fringes will be observed. The period of these fringes is a direct measure for the energy shift.

Optimal parameters of dressing lasers are obtained by solving for the eigenvectors and eigenvalues of the following matrix representation of an effective Hamiltonian within the quasi-resonant approximation involving the three states $|1\rangle$, $|2\rangle$ and $|3\rangle$ [53]:

$$\mathcal{H}\left(\Delta_2+\delta_{\mathrm{RM}}\right)/\hbar = \begin{pmatrix} -\mathrm{i}\Gamma_1 & \frac{1}{2}\Omega_{12} & 0 \\ \frac{1}{2}\Omega_{12} & -\mathrm{i}\Gamma_2+\Delta_1 & \frac{1}{2}\Omega_{23} \\ 0 & \frac{1}{2}\Omega_{23} & -\mathrm{i}\Gamma_3+\Delta_2+\delta_{\mathrm{RM}} \end{pmatrix} \tag{1}$$

with Rabi frequencies Ω_{12} and Ω_{23} as described in figure 2 and detunings of both dressing lasers Δ_1 and Δ_2 as defined in figure 2. $\hbar = h/(2\pi)$ denotes here the reduced Planck constant and δ_{RM} the interaction-

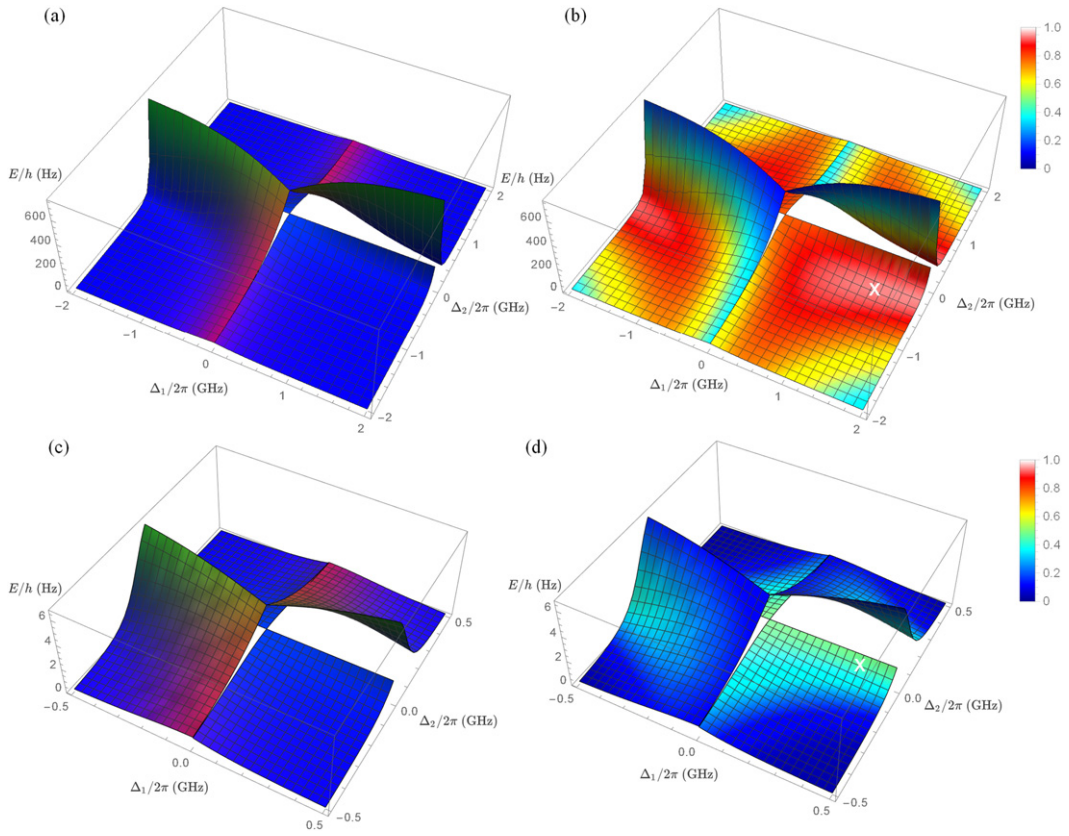

Figure 3. Energy shifts of the upper hyperfine component $|1\rangle$ of the electronic ground state of 87 Rubidium due to two photon dressing with $\Delta_1 = (E_2 - E_1)/\hbar - \omega_{12}^{\mathrm{L}}$ being the detuning of the 780 nm laser with respect to the $5^2P_{3/2}, F = 3$ state and $\Delta_2 = (E_3 - E_1)/\hbar - (\omega_{12}^{\mathrm{L}} + \omega_{23}^{\mathrm{L}})$ being the detuning of the two photon transition including the 480 nm laser to the Rydberg state. Positive values of Δ denote red detuning. First quadrant in each picture with values Δ_1 and $\Delta_2 > 0$ show the energy shifts of the dressed state with lowest energy, the second quadrant with $\Delta_1 < 0$ and $\Delta_2 > 0$ and the fourth quadrant with $\Delta_1 > 0$ and $\Delta_2 < 0$ correspond to the intermediate energy dressed eigenstate and the third quadrant with $\Delta_1 < 0$ and $\Delta_2 < 0$ depict the energy shifts of the dressed state with highest energy. (a) Energy shift E of the upper ground state due to a $\delta_{\mathrm{RB}}/(2\pi) = 1$ kHz shift in the Rydberg state with Rabi frequencies $\Omega_{12}/(2\pi) = 0.5$ GHz and $\Omega_{23}/(2\pi) = 1$ GHz. The sign of δ_{RB} is also reflected in the energy shift E. Blue/red/green colour intensity indicate dominating ground/intermediate/Rydberg state admixture to the corresponding dressed state. (b) Same data is plotted as in (a) but colour is now indicating the amplitude of the second Ramsey peak in relation to first Ramsey peak given by $\sum_i P_i\, \mathrm{e}^{-\Gamma_i/(E/\hbar)}$, with P_i being the probability of being in state $|i\rangle$. Thus it is better to choose detunings resulting in smaller energy shifts E (see white cross marker close to $\Delta_1/(2\pi) = 1.5$ GHz and $\Delta_2/(2\pi) = -0.2$ GHz. (c) Plot description is as in (a) but for a $\delta_{\mathrm{RM}}/(2\pi) = 10$ Hz shift in the Rydberg state plotted for a smaller detuning range and reduced Rabi frequencies of $\Omega_{12}/(2\pi) = 0.25$ GHz and $\Omega_{23}/(2\pi) = 0.5$ GHz. (d) Colours in plot are as described in (b) but for parameters given in (c). Note that optimal parameters depend on the expected signal strengths as can be seen by the shift of the white cross marker.

induced shift of the Rydberg state (possible chiral shifts of the other states are negligible by comparison in view of the large Rydberg dipole moments), with Γ_i being the decay rates. We assumed a conservative value of $\Gamma_1/(2\pi) = 1$ Hz for the upper hyperfine component of the electronic ground state due to collisions, $\Gamma_2/(2\pi) = 3.8 \times 10^7$ Hz and $\Gamma_3/(2\pi) = 1.4 \times 10^5$ Hz for a typical Rydberg state. If the Rydberg state shifts by δ_{RM}, we obtain the signal by comparing $\mathcal{H}(\Delta_2 + \delta_{\mathrm{RM}})$ with $\mathcal{H}(\Delta_2)$, which corresponds to the numerical derivative of $\mathcal{H}(\Delta_2)$ with respect to Δ_2 for δ_{RM} near zero. As a result, the energy shift of the upper ground state due to chiral interaction-induced shifts in the Rydberg state are obtained by comparing the eigenvalues of $\mathcal{H}(\delta_{\mathrm{RM}})$ to $\mathcal{H}(0)$. Figures 3(a) and (c) show that maximal energy shifts are obtained when Δ_2 is small. But this is not necessarily optimal as close to resonance admixtures of the high Rydberg state and the intermediate state lead to a strong reduction of the Ramsey fringe contrast. The relevant figure of merit is the decrease of the amplitude of the Ramsey fringe after a full oscillation period which is given by the interaction induced energy shift of the upper ground state. For Rabi frequencies of $\Omega_{12}/(2\pi) = 0.5$ GHz and $\Omega_{23}/(2\pi) = 1$ GHz and Rydberg frequency shifts of $\delta_{\mathrm{RM}}/2\pi = 1$ kHz, one finds optimal regions (see white shaded areas in figure 3(b)). Also note that for smaller Rydberg frequency shifts of 10 Hz, the dressing light intensities are halved, and different optimal detuning parameters have to be chosen (see green areas in figure 3(d)). The accuracy of the measured frequency shifts translated to the ground state manifold is limited by the T_1 and T_2^* times (longitudinal and effective transversal relaxation times) in the electronic ground-state hyperfine manifold.

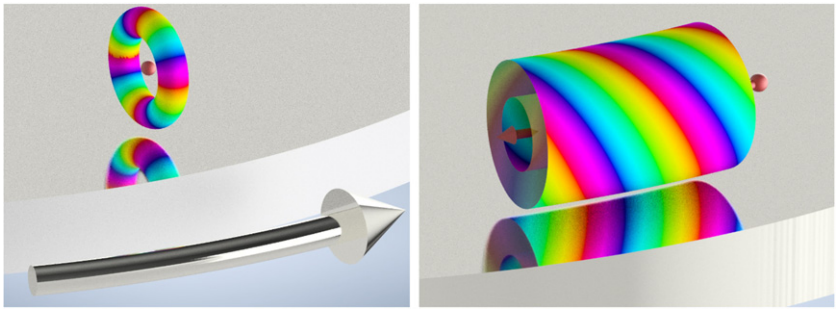

Figure 4. Enantiodiscriminatory interactions of Rydberg atoms: (left) the circular polarised electric dipole moment of a Rydberg atom above a disk rotating with velocity v generates a chiral wavefunction when seen from the rest frame of the rotating disc (right). The disc consists of a perfect chiral mirror, that experiences an enantiodiscriminatory interaction with the Rydberg atom. Upon reversing the circular polarisation, the opposite enantiomer is realised, reversing the sign of the interaction.

3. Chiral energy shifts in Rydberg atoms

Dispersion interactions between two objects can possess chiral components, as stated in the introduction. Curie's symmetry principle [54] dictates that for these to be enantiodiscriminatory, both interacting objects need to be chiral. In other words, a Rydberg atom can only acquire a chiral energy shift if itself exhibits handedness. This is typically not the case for Rydberg atoms and the associated dominant electric dipole–electric dipole interactions.

In this section, we present possible a solution to this challenge: a Rydberg atom prepared in a state with a nonvanishing x-component m of its orbital angular momentum, with x being arbitrarily chosen here as our quantisation axis, will preferentially or even exclusively undergo circularly polarised electric dipole transitions of a given rotation direction. If the atom moves parallel to the respective rotation axis, then its electric dipole moment maps out a corkscrew trajectory during a transition, with this corkscrew constituting a handed system (figure 4). This artificial chiral Rydberg system is transformed into its opposite enantiomer upon reversing either the direction of motion or the sign of the x-component of orbital angular momentum (and hence the rotation direction of the circular dipole transition). In the following, we will show that this system indeed exhibits discriminatory chiral dispersive energy shifts and estimate the order of magnitude of such shifts as induced by a chiral mirror (figure 4).

The interaction of a Rydberg atom A at instantaneous position $\boldsymbol{r}_{\mathrm{A}}$ with velocity $\boldsymbol{v}$ with the quantum electromagnetic field F in electric-dipole approximation is given by [18]

$$\hat{H}_{\mathrm{AF}} = -\hat{\boldsymbol{d}}\cdot\hat{\boldsymbol{E}}(\boldsymbol{r}_{\mathrm{A}}) - \hat{\boldsymbol{d}}\cdot\boldsymbol{v}\times\hat{\boldsymbol{B}}(\boldsymbol{r}_{\mathrm{A}}), \tag{2}$$

where $\hat{\boldsymbol{d}}$ is the atomic electric-dipole operator. Here, the first term is the usual electric-dipole coupling for an atom at rest and the velocity-dependent second term is the so-called Röntgen interaction [55]. The presence of this leading-order relativistic correction can be understood from the fact the electric field experienced by the moving atom in its own rest frame reads $\hat{\boldsymbol{E}}' = \hat{\boldsymbol{E}} + \boldsymbol{v}\times\hat{\boldsymbol{B}}$.

In order to induce discriminatory energy shifts, the mirror acting as a model for a general chiral system needs—again according to the Curie symmetry principle—to exhibit chiral properties corresponding to those of the Rydberg system. Such media are a special case (see equation (12) below) of arbitrary linear media, as represented by their frequency-dependent complex-valued nonlocal conductivity tensor $\boldsymbol{Q}(\boldsymbol{r},\boldsymbol{r}',\omega)$, where the quantized electromagnetic fields read [56]

$$\hat{\boldsymbol{E}}(\boldsymbol{r}) = \mathrm{i}\mu_0\int_0^\infty \mathrm{d}\omega\left[\mathbf{G}\star\hat{\boldsymbol{j}}_{\mathrm{N}}\right](\boldsymbol{r},\omega) + h.c., \tag{3}$$

$$\hat{\boldsymbol{B}}(\boldsymbol{r}) = \mu_0\int_0^\infty \frac{\mathrm{d}\omega}{\omega}\boldsymbol{\nabla}\times\left[\mathbf{G}\star\hat{\boldsymbol{j}}_{\mathrm{N}}\right](\boldsymbol{r},\omega) + h.c. \tag{4}$$

with the magnetic constant μ_0, +h.c. representing the Hermitian conjugate of the previous expression and $[\mathbf{T}\star\boldsymbol{v}](\boldsymbol{r}) = \int \mathrm{d}^3s\,\mathbf{T}(\boldsymbol{r},\boldsymbol{s})\cdot\boldsymbol{v}(\boldsymbol{s})$ and $[\mathbf{S}\star\mathbf{T}](\boldsymbol{r},\boldsymbol{r}') = \int \mathrm{d}^3s\,\mathbf{S}(\boldsymbol{r},\boldsymbol{s})\cdot\mathbf{T}(\boldsymbol{s},\boldsymbol{r}')$ denoting spatial convolutions for tensor and vector fields. Here, $\boldsymbol{G}$ is the classical Green tensor of rank 2 for the electromagnetic field which satisfies a generalized Helmholtz equation (with $\boldsymbol{\delta}$ denoting the Kronecker tensor of rank 2)

$$\left[\boldsymbol{\nabla}\times\boldsymbol{\nabla}\times - \frac{\omega^2}{c^2}\right]\mathbf{G} - \mathrm{i}\mu_0\omega[\mathbf{Q}\star\mathbf{G}] = \boldsymbol{\delta} \tag{5}$$

together with the boundary condition $\boldsymbol{G}(\boldsymbol{r},\boldsymbol{r}',\omega)\to\boldsymbol{0}$ for $|\boldsymbol{r}-\boldsymbol{r}'|\to\infty$. It fulfils the completeness relation

$$\mu_0\omega\mathbf{G}\star\mathcal{R}\mathrm{e}(\mathbf{Q})\star\mathbf{G}^\dagger=\mathcal{I}\mathrm{m}(\mathbf{G}), \tag{6}$$

where generalized real and imaginary parts of nonsymmetric tensor fields are defined as $\mathcal{R}\mathrm{e}(\mathbf{T})=[\mathbf{T}(\boldsymbol{r},\boldsymbol{r}')+\mathbf{T}^\dagger(\boldsymbol{r}',\boldsymbol{r})]/2$ and $\mathcal{I}\mathrm{m}(\mathbf{T})=[\mathbf{T}(\boldsymbol{r},\boldsymbol{r}')-\mathbf{T}^\dagger(\boldsymbol{r}',\boldsymbol{r})]/(2\mathrm{i})$; they reduce to ordinary (component wise) real and imaginary parts for symmetric tensor fields with $\boldsymbol{T}^\dagger(\boldsymbol{r}',\boldsymbol{r})=\boldsymbol{T}^*(\boldsymbol{r},\boldsymbol{r}')$. The noise currents $\hat{\boldsymbol{j}}_\mathrm{N}$ residing inside the present media can be expressed in terms of bosonic operators $\hat{\boldsymbol{f}}$: $\hat{\boldsymbol{j}}_\mathrm{N}=\sqrt{\hbar\omega/\pi}\mathbf{R}\star\hat{\boldsymbol{f}}$ with $\boldsymbol{R}$ being an arbitrary solution to $\mathbf{R}\star\mathbf{R}^\dagger=\mathcal{R}\mathrm{e}(\mathbf{Q})$.

With these preparations at hand, we can determine the dispersive energy shift of an atom in a given Rydberg state $|n\rangle$ due to its interaction with the quantum electromagnetic field in an arbitrary environment by following the original approach of Casimir and Polder [14]. Assuming the relevant body-assisted electromagnetic field to be in the vacuum state $|\{0\}\rangle$ [34], we calculate the energy shift

$$\Delta E=\sum_{I\neq\psi}\frac{\langle\psi|\hat{H}_\mathrm{AF}|I\rangle\langle I|\hat{H}_\mathrm{AF}|\psi\rangle}{E_\psi-E_I} \tag{7}$$

of the uncoupled state $|\psi\rangle=|i\rangle|\{0\}\rangle$ (in our case the Rydberg state $|i\rangle$ is a $\mathrm{n}^2\mathrm{D}_j$ state with $m_\ell=\pm2$) arising from the above atom–field dispersion interaction within leading, second-order perturbation theory. The relevant intermediate states $|I\rangle=|k\rangle|\mathbf{1}(\boldsymbol{r},\omega)\rangle$ involve single-photon states $|\mathbf{1}(\boldsymbol{r},\omega)\rangle=\boldsymbol{f}^\dagger(\boldsymbol{r},\omega)|\{0\}\rangle$, so the formal sum consists of a sum over atomic states $|k\rangle$ (in our case F and P states) and integrals over the respective position and frequency arguments. The relevant matrix elements of the two terms in the interaction (2) can be evaluated with the aid of the field expansions (3) and (4) together with the bosonic commutation relations:

$$\langle\{0\}|\langle i|-\hat{\boldsymbol{d}}\cdot\hat{\boldsymbol{E}}(\boldsymbol{r}_\mathrm{A})|k\rangle|\boldsymbol{1}(\boldsymbol{r},\omega)\rangle=-\mathrm{i}\mu_0\sqrt{\frac{\hbar\omega}{\pi}}\boldsymbol{d}_{ik}\cdot[\mathbf{G}\star\mathbf{R}]\,(\boldsymbol{r}_\mathrm{A},\boldsymbol{r},\omega), \tag{8}$$

$$\langle\{0\}|\langle i|-\hat{\boldsymbol{d}}\cdot\boldsymbol{v}\times\hat{\boldsymbol{B}}(\boldsymbol{r}_\mathrm{A})|k\rangle|\boldsymbol{1}(\boldsymbol{r},\omega)\rangle=-\mu_0\sqrt{\frac{\hbar}{\pi\omega}}\boldsymbol{d}_{ik}\cdot\boldsymbol{v}\times(\boldsymbol{\nabla}_\mathrm{A}\times[\mathbf{G}\star\mathbf{R}])\,(\boldsymbol{r}_\mathrm{A},\boldsymbol{r},\omega) \tag{9}$$

with electric dipole matrix elements $\boldsymbol{d}_{ik}=\langle i|\hat{\boldsymbol{d}}|k\rangle$. We insert these results and their complex conjugates into the above energy shift and retain only the leading-order chiral contributions which are due to cross-terms of electric-dipole and Röntgen couplings. Using the completeness relation (6), we find

$$\begin{aligned}\hbar\delta_\mathrm{RM}=\frac{\mu_0}{\pi}\sum_{k\neq i}\mathcal{P}\int_0^\infty\mathrm{d}\omega\,\frac{\omega}{\omega-\omega_{ik}}\mathrm{Re}\,[\boldsymbol{v}\times\boldsymbol{d}_{ki}\cdot\boldsymbol{\nabla}\times\mathbf{G}(\boldsymbol{r},\boldsymbol{r}_\mathrm{A},\omega)\cdot\boldsymbol{d}_{ik}\\-\boldsymbol{v}\times\boldsymbol{d}_{ik}\cdot\boldsymbol{\nabla}\times\mathbf{G}(\boldsymbol{r},\boldsymbol{r}_\mathrm{A},\omega)\cdot\boldsymbol{d}_{ki}]_{\boldsymbol{r}=\boldsymbol{r}_\mathrm{A}}\end{aligned} \tag{10}$$

with atomic transition frequencies $\omega_{ik}=(E_i-E_k)/\hbar$, and the Cauchy principal value $\mathcal{P}$. As a consistency check, we note that the above energy shift hence vanishes when (i) the dipole moments are linearly polarised ($\boldsymbol{d}_{ik}=\boldsymbol{d}_{ki}$) and hence the atom does not exhibit handedness. Upon splitting the Green tensor $\boldsymbol{G}=\boldsymbol{G}^{(0)}+\boldsymbol{G}^{(1)}$ into its bulk and scattering parts $\boldsymbol{G}^{(0)}$ and $\boldsymbol{G}^{(1)}$, respectively, the former does not contribute due to the symmetry $\boldsymbol{G}^{(0)}(\boldsymbol{r},\boldsymbol{r}')=\boldsymbol{G}^{(0)}(\boldsymbol{r}',\boldsymbol{r})$. After applying contour-integration techniques and only retaining the dominant resonant contribution from the pole at $\omega=\omega_{ik}$, we find

$$\hbar\delta_\mathrm{RM}=\mu_0\sum_{k<n}\omega_{ik}\left[\boldsymbol{v}\times\boldsymbol{d}_{ik}\cdot\boldsymbol{\nabla}\times\mathrm{Re}\;\mathbf{G}^{(1)}(\boldsymbol{r}_\mathrm{A},\boldsymbol{r}_\mathrm{A},\omega_{ik})\cdot\boldsymbol{d}_{ki}+c.c.\right]. \tag{11}$$

Finally, we apply this general result to our specific geometry of a Rydberg atom with a single circularly polarised transition $\boldsymbol{d}_{ki}=(d_{ki}/\sqrt{2})(\boldsymbol{e}_y+\mathrm{i}\boldsymbol{e}_z)$ rotating in the yz plane travelling with a velocity $\boldsymbol{v}=v\boldsymbol{e}_x$ parallel to the rotation axis at position $\boldsymbol{r}_\mathrm{A}=z_\mathrm{A}\boldsymbol{e}_z$ above a perfectly reflecting chiral mirror in the $z=0$ plane (see figure 4). Whereas the description above was general, we now introduce chirality by the use of the scattering Green tensor of the of a chiral mirror as given by [28]

$$\mathbf{G}^{(1)}(\boldsymbol{r},\boldsymbol{r}',\omega)=\frac{\mathrm{i}}{8\pi^2}\int\frac{\mathrm{d}^2k^\parallel}{k^\perp}\,\mathrm{e}^{\mathrm{i}\boldsymbol{k}^\parallel(\boldsymbol{r}-\boldsymbol{r}')+\mathrm{i}k^\perp(z+z')}\sum_{\sigma,\sigma'=\mathrm{s,p}}r_{\sigma\sigma'}\boldsymbol{e}_{\sigma+}\boldsymbol{e}_{\sigma'-}, \tag{12}$$

where $\boldsymbol{e}_{\sigma\pm}$ are unit vectors for incident $(-)$ and reflected $(+)$ s- and p-polarised waves and $r_{\sigma\sigma'}$ are the respective reflection coefficients. For a perfect chiral mirror in particular, which rotates the polarisation of

incoming light by $\pi/2$ upon reflection, we have $r_{\rm ss} = r_{\rm pp} = 0$, $r_{\rm sp} = -r_{\rm ps} \equiv r$, so that the reflection matrix in the s, p-basis reads

$$R = \begin{pmatrix} 0 & r \\ -r & 0 \end{pmatrix}. \tag{13}$$

Introducing unit vectors for incoming and outgoing right- (r) and left- (l) circularly polarised waves according to

$$\begin{pmatrix} \boldsymbol{e}_{\rm r\pm} \\ \boldsymbol{e}_{\rm l\pm} \end{pmatrix} = U_{\pm} \begin{pmatrix} \boldsymbol{e}_{\rm s\pm} \\ \boldsymbol{e}_{\rm p\pm} \end{pmatrix} \tag{14}$$

with

$$U_{\pm} = \frac{1}{\sqrt{2}} \begin{pmatrix} 1 & \pm{\rm i} \\ 1 & \mp{\rm i} \end{pmatrix} \tag{15}$$

the reflection matrix in the r, l-basis is seen to be diagonal,

$$R' = U_{+}^{\dagger{\rm T}} \cdot R \cdot U_{-}^{\dagger} = \begin{pmatrix} {\rm i}r & 0 \\ 0 & -{\rm i}r \end{pmatrix}, \tag{16}$$

showing that this mirror is handedness-preserving. Handedness-preserving mirrors can be realized by placing a 2D fish-scale [57] or split-ring [58] metamaterial at sub-wavelength distance from a metallic mirror, where reflectivities in the range 80%–90% have been reported.

Evaluating the curl of the Green tensor by means of the orthonormality relation $\boldsymbol{e}_{\rm p\pm} \times \boldsymbol{e}_{\rm s\pm} = \boldsymbol{k}_{\pm}/k_{\pm}$ with $\boldsymbol{k}_{\pm} = \boldsymbol{k}_{\parallel} \pm k^{\perp}\boldsymbol{e}_z$ and carrying out the integral over the parallel component of the wave vector $\boldsymbol{k}^{\parallel}$, one easily finds

$$\boldsymbol{\nabla} \times \mathbf{G}^{(1)}(\boldsymbol{r}_{\rm A}, \boldsymbol{r}_{\rm A}, \omega_{ik}) = -\frac{{\rm i}cr}{32\pi\omega_{ik} z_{\rm A}^3} \begin{pmatrix} 1 & 0 & 0 \\ 0 & 1 & 0 \\ 0 & 0 & 2 \end{pmatrix} \tag{17}$$

in the nonretarded regime $z_{\rm A} \ll c/\omega_{ki}$, typically valid for Rydberg atoms. Combining this with the above choices for velocity and dipole moments and fixing the phase upon reflection to be $r = {\rm e}^{{\rm i}\pi/2} = {\rm i}$, we obtain

$$\hbar\delta_{\rm RM} = \frac{3v d_{ki}^2}{32\pi\varepsilon_0 c z_{\rm A}^3}. \tag{18}$$

Indeed, a moving Rydberg atom with a circular dipole transition exhibits a chiral energy shift near a nonreciprocal mirror. As required, the detected energy shift changes sign upon replacing the Rydberg system with its opposite enantiomer by reversing either the velocity ($\boldsymbol{v} \mapsto -\boldsymbol{v}$) or the rotation of the dipole transition ($\boldsymbol{d}_{ki} \mapsto \boldsymbol{d}_{ki}^{*}$).

To estimate the order of magnitude of the discriminatory chiral energy shift, let us compare it with the ordinary resonant electric energy shift [15, 59]

$$\hbar\delta = \frac{3d_{ki}^2}{128\pi\varepsilon_0 z_{\rm A}^3} \tag{19}$$

of a stationary Rydberg atom at distance $z_{\rm A}$ from a perfectly conducting plate which arises from the first term in the atom-field coupling. The discriminatory term displays the same distance dependence as the standard electric energy shift. Being a leading-order relativistic correction, it is smaller than the latter by a factor $4v/c$ which for a 10 cm sized disk rotating at 100 kRPM achieving velocities of 10^3 m s^{-1} is of the order 10^{-5}. Given that electric frequency shifts of Rydberg atoms can be of the order of 10^9 Hz at a distance of 1 μm [35], we estimate the chiral frequency shifts to be of the order of 10^4 Hz. It can be enhanced by further reducing the distance (where higher-order multipole moments need to be taken into account) or by enhancing the atom-field coupling using microwave cavities. Note that our highly idealised calculation can only provide a rough estimate of the order of magnitude to be expected. A full quantitative analysis for a given metamaterial mirror would require a numerical solution of the Maxwell equations for the respective structure in order to account for the angle-dependence of the reflectivities. This could be implemented by the recently developed Casimir numerics [60].

The predicted linear scaling with velocity v is only valid for nonrelativistic speeds. Geometrically, the slope of the helix traced out by the electric dipole vector in figure 4 is $h/(2\pi r) = v/(a_n\omega_{ki})$ with pitch $h = 2\pi v/\omega_{ki}$ and radius $r = a_n$ (radius of the Rydberg orbital). The slope is very small for Rydberg atoms at moderate speeds, as can be seen by estimating $a_n \approx a_0 n^2$ and $\omega_{ki} \approx 2E_{\rm R}/(\hbar n^3)$, hence $a_n\omega_{ki} \approx 2 \times 10^6 ({\rm m\ s^{-1}})/n$.

4. Conclusion

Rydberg atoms are well suited for implementing tailored quantum sensors able to measure small interaction-induced energy shifts. By combining sensitivity with the stability offered by the hyperfine states in the ground state manifold we can implement a sensitive interferometer which should be able to sense motion-induced chirality in achiral atoms and find signatures of Casimir–Polder quantum friction. We give estimates of the expected interaction strength by calculating the interaction with a chiral mirror.

Acknowledgments

We are grateful for discussions with T Momose, A Salam, F Suzuki. This work has been funded by the German Research Foundation (DFG, Project No. 328961117-SFB 1319 ELCH, Grant BU 1803/3-1476, S.Y.B.).

Data availability statement

The data generated and/or analysed during the current study are not publicly available for legal/ethical reasons but are available from the corresponding author on reasonable request.

ORCID iDs

R Berger https://orcid.org/0000-0002-9107-2725
K Singer https://orcid.org/0000-0001-9726-0367

References

[1] Jau Y-Y, Hankin A M, Keating T, Deutsch I H and Biedermann G W 2016 *Nat. Phys.* **12** 71–4
[2] Mitra A, Martin M J, Biedermann G W, Marino A M, Poggi P M and Deutsch I H 2020 *Phys. Rev.* A **101** 030301
[3] Arias A, Lochead G, Wintermantel T M, Helmrich S and Whitlock S 2019 *Phys. Rev. Lett.* **122** 053601
[4] Adams C S, Pritchard J D and Shaffer J P 2019 *J. Phys. B: At. Mol. Opt. Phys.* **53** 012002
[5] Weidemüller M, Singer K, Reetz-Lamour M, Amthor T and Marcassa L G 2005 *AIP Conf. Proc.* **770** 157–63
[6] Weidemüller M, Reetz-Lamour M, Amthor T, Deiglmayr J, Singer K and Marcassa L G 2005 *Interactions in an Ultracold Gas of Rydberg Atoms* (Singapore: World Scientific) pp 264–74
[7] Singer K, Reetz-Lamour M, Tscherneck M, Föiling S and Weidemüller M 2005 *A Interactions in Trapped Atomic Gases* (New York: Wiley) ch 15 pp 402–4
[8] Singer K, Reetz-Lamour M, Amthor T, Marcassa L G and Weidemüller M 2004 *Phys. Rev. Lett.* **93** 163001
[9] Singer K, Stanojevic J, Weidemüller M and Côté R 2005 *J. Phys. B: At. Mol. Opt. Phys.* **38** S295–307
[10] Singer K, Reetz-Lamour M, Amthor T, Fölling S, Tscherneck M and Weidemüller M 2005 *J. Phys. B: At. Mol. Opt. Phys.* **38** S321–32
[11] Ramsey N F 1950 *Phys. Rev.* **78** 695–9
[12] Ivannikov V and Sidorov A I 2018 *J. Phys. B: At. Mol. Opt. Phys.* **51** 205002
[13] London F 1930 *Z. Phys.* **63** 245
[14] Casimir H B G and Polder D 1948 *Phys. Rev.* **73** 360
[15] Lennard-Jones J E 1932 *Trans. Faraday Soc.* **28** 333
[16] Agarwal G S 1975 *Phys. Rev.* A **11** 243
[17] Wylie J M and Sipe J E 1985 *Phys. Rev.* A **32** 2030
[18] Buhmann S Y, Knöll L, Welsch D G and Ho D T 2004 *Phys. Rev.* A **70** 052117
[19] Woods L, Dalvit D A R, Tkatchenko A, Rodriguez-Lopez P, Rodriguez A W and Podgornik R 2016 *Rev. Mod. Phys.* **88** 045003
[20] Kenneth O, Klich I, Mann A and Revzen M 2002 *Phys. Rev. Lett.* **89** 033001
[21] Henkel C and Joulain K 2005 *Europhys. Lett.* **72** 929
[22] Rosa F S S, Dalvit D A R and Milonni P W 2008 *Phys. Rev. Lett.* **100** 183602
[23] Jenkins J K, Salam A and Thirunamachandran T 1994 *Phys. Rev.* A **50** 4767
[24] Craig D P and Thirunamachandran T 1999 *Theor. Chem. Acc.* **102** 112–20
[25] Butcher D T, Buhmann S Y and Scheel S 2012 *New J. Phys.* **14** 113013
[26] Barcellona P, Safari H, Salam A and Buhmann S Y 2017 *Phys. Rev. Lett.* **118** 193401
[27] Grushin A G and Cortijo A 2011 *Phys. Rev. Lett.* **106** 020403
[28] Fuchs S, Crosse J and Buhmann S Y 2017 *Phys. Rev.* A **95** 023805
[29] Fuchs S, Lindel F, Krems R V, Hanson G W, Antezza M and Buhmann S Y 2017 *Phys. Rev.* A **96** 062505
[30] Gallagher T F 2005 *Rydberg Atoms* (Cambridge: Cambridge University Press)
[31] Yerokhin V, Buhmann S, Fritzsche S and Surzhykov A 2016 *Phys. Rev.* A **94** 032503
[32] Sukenik C I, Boshier M G, Cho D, Sandoghdar V and Hinds E A 1993 *Phys. Rev. Lett.* **70** 560
[33] Marrocco M, Weidinger M, Sang R T and Walther H 1998 *Phys. Rev. Lett.* **81** 5784
[34] Ellingsen S Å, Buhmann S Y and Scheel S 2010 *Phys. Rev. Lett.* **104** 223003

[35] Crosse J, Ellingsen S Å, Clements K, Buhmann S Y and Scheel S 2010 *Phys. Rev.* A **82** 010901
[36] Yang B, Zhang B, Liu Z and Yao H 2019 *J. Phys. B: At. Mol. Opt. Phys.* **52** 095501
[37] Block J and Scheel S 2019 *Phys. Rev.* A **100** 062508
[38] Antezza M, Braggio C, Carugno G, Noto A, Passante R, Rizzuto L, Ruoso G and Spagnolo S 2014 *Phys. Rev. Lett.* **113** 023601
[39] Barron L D 2013 *Rend. Lincei* **24** 179–89
[40] Hammer N I, Gao F, Pagni R M and Compton R N 2002 *J. Chem. Phys.* **117** 4299–305
[41] Canaguier-Durand A, Hutchison J A, Genet C and Ebbesen T W 2013 *New J. Phys.* **15** 123037
[42] Cameron R P, Barnett S M and Yao A M 2014 *New J. Phys.* **16** 013020
[43] Pendry J B 1997 *J. Phys.: Condens. Matter* **9** 10301
[44] Pendry J B 2010 *New J. Phys.* **12** 033028
[45] Milton K, Høye J and Brevik I 2016 *Symmetry* **8** 29
[46] Volokitin A I and Persson B N J 2007 *Rev. Mod. Phys.* **79** 1291
[47] Dedkov G V and Kyasov A A 2008 *J. Phys.: Condens. Matter* **20** 354006
[48] Intravaia F, Behunin R and Dalvit D 2014 *Phys. Rev.* A **89** 050101
[49] Scheel S and Buhmann S 2009 *Phys. Rev.* A **80** 042902
[50] Klatt J, Bennett R and Buhmann S 2016 *Phys. Rev.* A **94** 063803
[51] Farías M B, Lombardo F C, Soba A, Villar P I and Decca R S 2020 *npj Quantum Inf.* **6** 25
[52] Genov G T, Schraft D, Halfmann T and Vitanov N V 2014 *Phys. Rev. Lett.* **113** 043001
[53] Shore B W 1990 *The Theory of Coherent Atomic Excitation* (*Simple Atoms and Fields* vol 1) (New York: Wiley)
[54] Curie P 1894 *J. Phys.: Theor. Appl.* **3** 393
[55] Baxter C, Babiker M and Loudon R 1993 *Phys. Rev.* A **47** 1278
[56] Buhmann S Y, Butcher D T and Scheel S 2012 *New J. Phys.* **14** 083034
[57] Fedotov V A, Rogacheva A V, Zheludev N I, Mladyonov P L and Prosvirnin S L 2006 *Appl. Phys. Lett.* **88** 091119
[58] Plum E and Zheludev N I 2015 *Appl. Phys. Lett.* **106** 221901
[59] Buhmann S 2013 *Dispersion Forces II: Many-Body Effects, Excited Atoms, Finite Temperature and Quantum Friction* (Berlin: Springer)
[60] Reid M H, Rodriguez A W, White J and Johnson S G 2009 *Phys. Rev. Lett.* **103** 040401